Available online at www.sciencedirect.com
ScienceDirect
Ceramics International 37 (2011) 525–531
CERAMICS INTERNATIONAL
www.elsevier.com/locate/ceramint

Preparation of Y_2O_3:Eu^{3+} nanopowders via polymer complex solution method and luminescence properties of the sintered ceramics

Radenka M. Krsmanović [1,*], Željka Antić, Marko G. Nikolić, Miodrag Mitrić, Miroslav D. Dramićanin

Vinča Institute of Nuclear Sciences, University of Belgrade, P.O. Box 522, 11001 Belgrade, Serbia

Received 23 July 2010; received in revised form 9 September 2010; accepted 22 September 2010
Available online 29 October 2010

Abstract

Herein we presented polymer complex solution method for production of well crystalline europium doped Y_2O_3 nanopowders. Polyethylene glycol (PEG) of five different molecular weights is used both as a fuel and as a nucleation agent for the crystallization. Powders were cold-pressed and sintered to obtain ceramics. SEM images taken from ceramic pellets indicate formation of a dense structure, with a pronounced grain growth and low pore concentration. Luminescence emission spectra of powders and ceramics are similar, and in good agreement with theoretical data. Lifetimes of Eu^{3+} $^5D_0$ level in nanocrystalline powders are higher compared to one observed in bulk, confirming in this case theory of lifetime lengthening in nanophosphors due to the change of effective refraction index. As expected, lifetime values in ceramic samples decrease toward the value in bulk Y_2O_3. The optical filling factor is calculated from observed decay times, providing a measure of discrepancy between powder and bulk state regarding their luminescent properties.

Keywords: A. Powders-chemical preparation; B. Grain size; C. Optical properties; D. Y_2O_3

1. Introduction

Phosphors are materials that absorb energy and subsequently emit it as light by luminescence [1]. Most of them are composed of a transparent host and an activator, typically a transition metal or rare earth ion. Among them, oxide phosphors are found to be suitable for field emission (FED), vacuum fluorescent (VFD), electroluminescent (EL) and plasma panel (PDP) display devices. Phosphors based on Eu^{3+} doped rare-earth (RE) sesquioxides, such as yttrium and gadolinium oxides, are well-known materials widely used to provide red light emission for modern optoelectronic devices and their investigation is still of great interest [2–6]. Regarding phosphors for scintillating applications they are the first choice for sintered scintillators [7].

Traditionally, RE_2O_3 phosphors are prepared by a solid state reaction method starting with a mechanical mixing of precursor oxides, followed by a ball-milling and calcination. Common problems of this method are poor sintering behavior of the material, nonhomogeneity and imprecise control of cation stoichiometry and high processing temperature [8].

Here we present a polymer complex solution (PCS) method as a low temperature synthesis procedure for production of Y_2O_3-based phosphor powders. The utility of used polymeric approach is two-folded: (i) the chelating of the cations onto the polymer chains is provided and (ii) the development of extremely high-viscosity polymeric raisins occurs during the gelation process, resulting in very low cation mobility. However, the organic precursor, in our case polyethylene glycol (PEG), not only works as a chelating agent and resin vehicle, but also as an organic fuel to provide combustion heat for the calcination [9]. On ignition, an intimate oxide mixture is

* Corresponding author at: Laboratory for Radiation Chemistry and Physics, Vinca Institute of Nuclear Sciences, Mike Petrovića Alasa 12-14, 11001 Belgrade, Serbia. Tel.: +381 11 3408 195;
fax: +381 11 3408 607/+39 0831 201581.
E-mail addresses: radenka@vinca.rs, radenka@gmail.com (R.M. Krsmanović).
[1] Current address: ENEA - Italian National Agency for New Technologies, Energy and the Environment Advanced Physical Technologies and New Materials Dept., S.S. 7 - Km 714, 72100 Brindisi, Italy.

0272-8842/$36.00
doi:10.1016/j.ceramint.2010.09.040

obtained and considerable mass is lost as the polymer matrix is burned away. In this way the PCS method keeps the main advantages of combustion method, which are simplicity of process and equipment and low cost of used materials [10,11].

The main goal of this study was to determine the influence of different molecular weight of used PEGs on the structural, morphological and luminescent characteristics of the synthesized powders, and from them subsequently prepared ceramics by cold-pressing and sintering.

2. Materials and methods

2.1. Samples preparation

Five samples of Y_2O_3 metal oxide powders doped with 3 at% of Eu^{3+} were prepared employing polyethylene glycols of different average molecular weights (200, 2000, 4000, 12000 and 20000, all Alfa Aesar). Water solutions of stoichiometric quantities of Y and Eu-nitrate were prepared by dissolving appropriate quantities of Y_2O_3 and Eu_2O_3 (both Alfa Aesar, 99.9%) in hot nitric acid. In so obtained solutions PEG was added in 1:1 mass ratio to the starting oxides. Metal-PEG solution is stirred at 80 °C for 2 h forming metal-PEG solid complex which is then combusted at 800 °C in air and finally calcinated at the same temperature for 2 h. Synthesized powders were cold-pressed under the pressure of 700 MPa and obtained pellets are subsequently sintered in a conventional oven at 1200 °C for 18 h aiming to produce translucent high density ceramics.

2.2. Experimental details

X-ray diffraction measurements were obtained on a Philips PW 1050 instrument, using Ni filtered Cu $K_{\alpha 1,2}$ radiation. Diffraction data were recorded in a 2θ range from 10° to 120° counting for 15 s in 0.02° steps. Structure analysis was performed using Kolariet computer software [12] based on a Rietveld full profile refinement method. The microstructure for powders and ceramic pellets was investigated with scanning electron microscope JEOL JSM 6460 LV. The luminescence measurements were performed at room temperature on the Fluorolog-3 Model FL3-221 spectroflurometer system (Horiba Jobin-Yvon), utilizing 450-W Xenon lamp as excitation source for emission measurements and Xenon-Mercury pulse lamp for lifetime measurements. TBX-04-D PMT detector was used for both lifetime and steady state acquisitions.

3. Results and discussion

3.1. Structural and morphological analysis

It is well known that Y_2O_3 crystallizes in a cubic bixbyte type of structure – space group Ia $\bar{3}$ (No. 206). In this structural type cations occupy two different crystallographic positions 8b (1/4, 1/4, 1/4) with point symmetry $\bar{3}$ (S_6, C_{3i}) and 24d (x, 0, 1/4) with point symmetry 2 (C_2). For both sites cations are octahedrally coordinated while the oxygen ion, in the general 48e position, is tetrahedrally surrounded [13]. Elementary cell is body centered with 16 formulae units. The schematic representation of Y_2O_3 structure is given in Fig. 1a.

Our previous investigation show that using polymer complex solution synthesis approach well crystalline, europium doped yttrium samples can be obtained [14]. In this study XRD measurements confirmed that pure Y_2O_3 phase has been obtained for all samples produced using PEGs with different average molecular weight (200, 2000, 4000, 12000 and 20000). Measured XRD pattern together with the final Rietveld plot for the Y_2O_3:Eu^{3+} powder obtained using PEG 200 is given in Fig. 1b with the relevant structural and microstructural data (crystal coherence size, unit cell parameter, ion coordinates and microstrain value).

Microstructure characterization of studied samples was carried out by SEM and selected images are presented in Fig. 2.

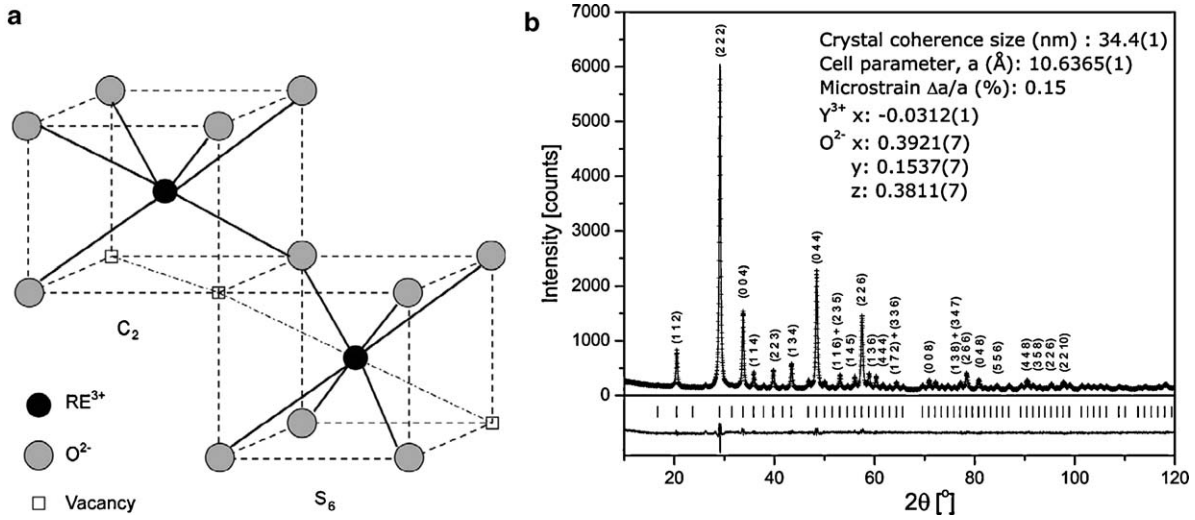

Fig. 1. (a) Schematic presentation of Y_2O_3 crystal lattice. (b) Observed (crosses), calculated (solid line) and difference XRD pattern of Y_2O_3:Eu^{3+} powder sample produced with PEG 200; the diffraction peaks are indexed according to JCPDS card no. 41-1105. Crystallographic data obtained from the Rietveld analysis are shown as inset. Thick marks denote the peak positions of Bragg reflections of Y_2O_3 cubic phase.

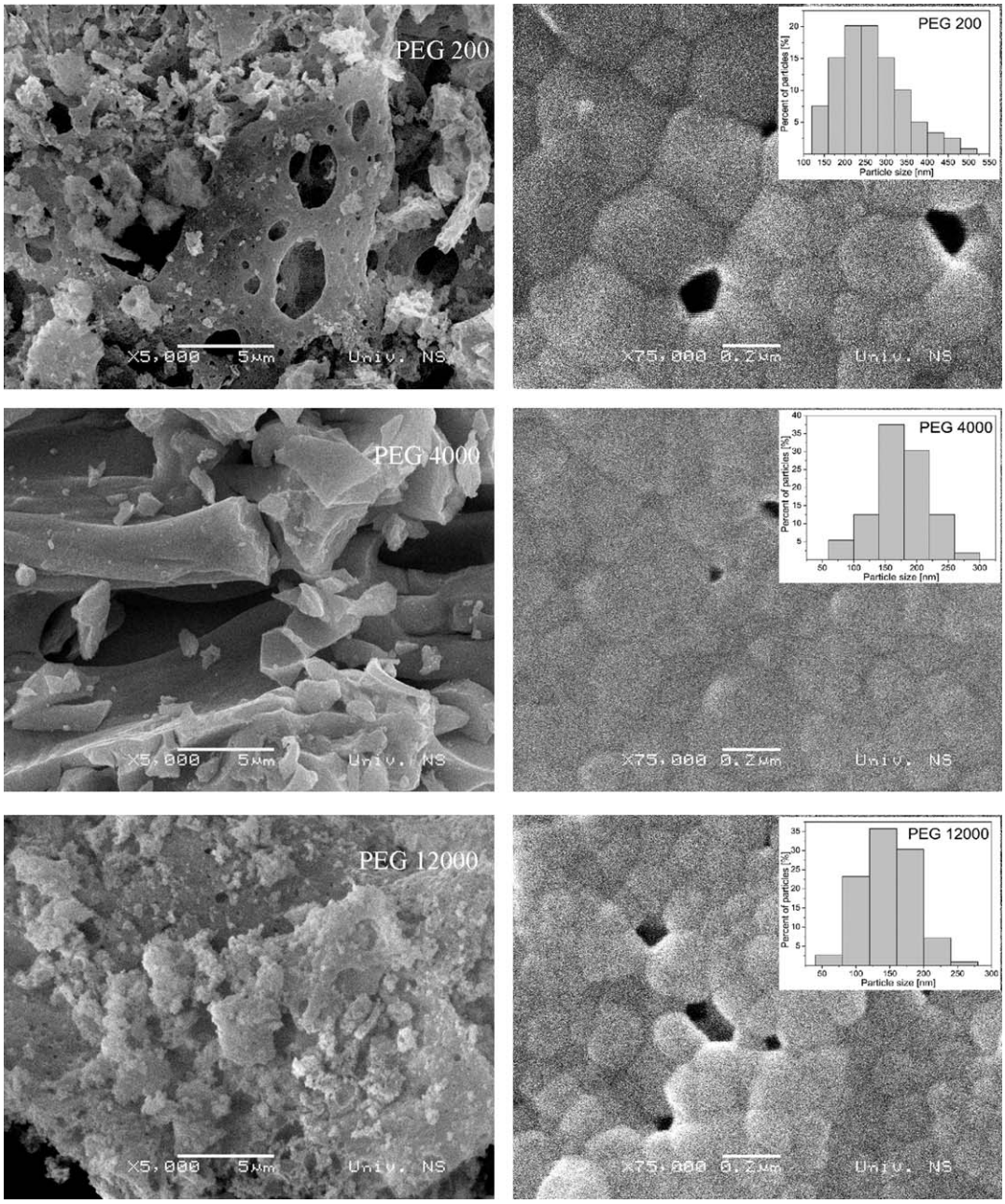

Fig. 2. SEM images of powders (left, marker bar is 5 μm) and pellets (right, marker bar is 0.2 μm) samples. The size distribution of observed grains is presented with histograms.

SEM observations of powders clearly show that powder structures differs with polyethylene glycol's average molecular weight, i.e. with different polymer chain length. For PEG 200 and 2000 one can notice puffed structure typical for materials obtained with standard combustion synthesis. On the other hand, for PEG 4000, with longer polymer chains, microstructure differs and material consists of large and dense, micron size ''chunks''. PEG 12000 and 20000 samples are similar to PEG 200 and 2000 but with more pronounced densification. SEM images taken from the pellets indicated the formation of a dense structure, with a marked grain growth and low pore concentration. We observed that the variation of grain sizes is a direct function of PEG molecular weight: for longer polymer chains grains are smaller in size (see histograms in Fig. 2). The largest grains, with average size of 250 nm, are observed in PEG 200 pellet, and the smallest for PEG 20000 of about 130 nm.

3.2. Optical properties

Luminescence emission spectra of all Y_2O_3:Eu^{3+} nanopowders and derived ceramic pellets are presented in Fig. 3. Five characteristic bands centered at around 580, 593, 610, 650 and 708 nm, associated to $^5D_0 \rightarrow {}^7F_i$ (i = 0, 1, 2, 3 and 4) spin forbidden f-f transitions, respectively, can be observed. The $^5D_0 \rightarrow {}^7F_1$ transition is the parity-allowed magnetic dipole transition (ΔJ = 1) and its intensity does not vary with the host. On the contrary, the $^5D_0 \rightarrow {}^7F_2$ electric dipole transition

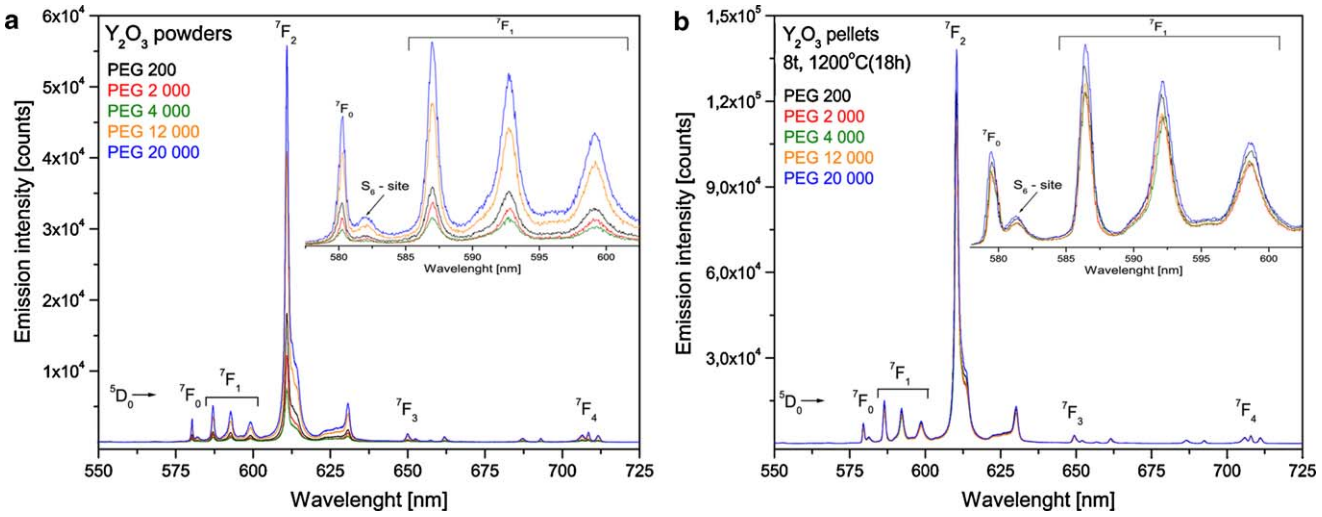

Fig. 3. Luminescence emission spectra for Y_2O_3:Eu^{3+} powder (a) and pellet (b) samples, obtained under excitation of 467 nm. Enlarged parts of emission spectra (575–605 nm) with indicated emission lines arising from europium ions residing in S_6 sites are given as insets. (For interpretation of the references to color, the reader is referred to the web version of the article.)

($\Delta J = 2$) is very sensitive to the local environment around Eu^{3+}, and its intensity depends on the symmetry of the crystal field around the europium ion. The asymmetry ratio of the integrated intensity of the $^5D_0 \rightarrow {}^7F_2$ and $^5D_0 \rightarrow {}^7F_1$ transitions can be considered as indicative of the asymmetry of the coordination environment around the Eu^{3+} ion, and is given by Eq. (1):

$$R = \frac{I(^5D_0 \rightarrow {}^7F_2)}{I(^5D_0 \rightarrow {}^7F_1)} \quad (1)$$

Values of R factor, calculated for both powders and pellets are presented in Tables 1 and 2. We observed that R factor values are higher for the powder samples, indicating that pellets have lower asymmetry of the coordination environment. This is a direct consequence of the structural consolidation due to the applied treatment – loading and annealing.

Part of the spectra taken from 575 to 605 nm is given as insert in both graphs to closely examine splitting of the $^7F_1$ manifold. One can notice two peaks, one originating from $^5D_0 \rightarrow {}^7F_0$ transition of Eu^{3+} located in C_2 site at around 580 nm and the other from $^5D_0 \rightarrow {}^7F_1$ transition of Eu^{3+} located in S_6 site at around 582 nm. For europium ions residing in centrosymmetric S_6 site only weak magnetic dipole transitions are possible, therefore only a low intensity luminescence peak from S_6 site may be observed, while all other luminescence comes from europium ions residing in C_2 site. Exact positions of these lines are given in Tables 1 and 2, for powder and pellet samples respectively. Stark components of the $^7F_1$ manifold are clearly visible and their values together with values of the maximum splitting ΔE are also presented in Tables 1 and 2. These results proved a good agreement with theoretical data indicating that well crystalline Y_2O_3:Eu^{3+} samples are obtained [15]. ΔE values for the ceramic samples are almost identical with powder ones, showing equal strength of the crystal field acting on europium ions in both types of samples [15], indicating in this way that no change in Eu–O distances has occurred during transformation from powders to ceramics. All these results confirmed that the ceramic pellets retained good luminescent properties of the starting nanocrystalline powder.

In Fig. 4 are presented fluorescence decay curves of the $^5D_0$ emitting level obtained for powder and pellet samples under the excitation of 467 nm ($\lambda_{em} = 611$ nm). Calculated lifetime

Table 1
Selected parameters obtained after luminescence measurements on Y_2O_3:Eu^{3+} powder samples.

Y_2O_3:Eu^{3+} powder	PEG 200	PEG 2000	PEG 4000	PEG 12000	PEG 20000
$^5D_0 \rightarrow {}^7F_0$ C_2 site (nm)	580.2	580.3	580.2	580.3	580.3
$^5D_0 \rightarrow {}^7F_1$ S_6 site (nm)	581.9	582.1	581.9	582.1	581.9
$^5D_0 \rightarrow {}^7F_1$ C_2 site (nm)	587 592.7 599.1	587 592.8 599.1	587 592.6 599.2	587 592.7 599.2	586.9 592.7 599.2
R	14.9	13.7	12.4	14.5	14.2
ΔE (cm^{-1})	344	341	349	342	347
ΔE_{theor} [15] (cm^{-1})			355		
τ ($^5D_0 \rightarrow {}^7F_2$) (ms)	1.6	1.4	1.2	1.5	1.4

Table 2
Selected parameters obtained after luminescence measurements on Y_2O_3:Eu^{3+} pellet samples.

Y_2O_3:Eu^{3+} pellets	PEG 200	PEG 2000	PEG 4000	PEG 12000	PEG 20000
$^5D_0 \rightarrow {}^7F_0C_2$ site (nm)	579.5	579.5	579.4	579.6	579.4
$^5D_0 \rightarrow {}^7F_1$ S_6 site (nm)	581.4	581.3	581.4	581.4	581.3
$^5D_0 \rightarrow {}^7F_1$ C_2 site (nm)	586.3 592.1 598.7	586.3 592.1 598.7	586.4 592.3 598.5	586.4 592.1 598.6	586.5 592.1 598.7
R	11.9	12.4	12.7	12.3	12.6
ΔE (cm^{-1})	352	351	345	346	348
ΔE_{theor} [15] (cm^{-1})			355		
τ($^5D_0 \rightarrow {}^7F_2$) (ms)	1.1	1.1	1.1	1.1	1.1

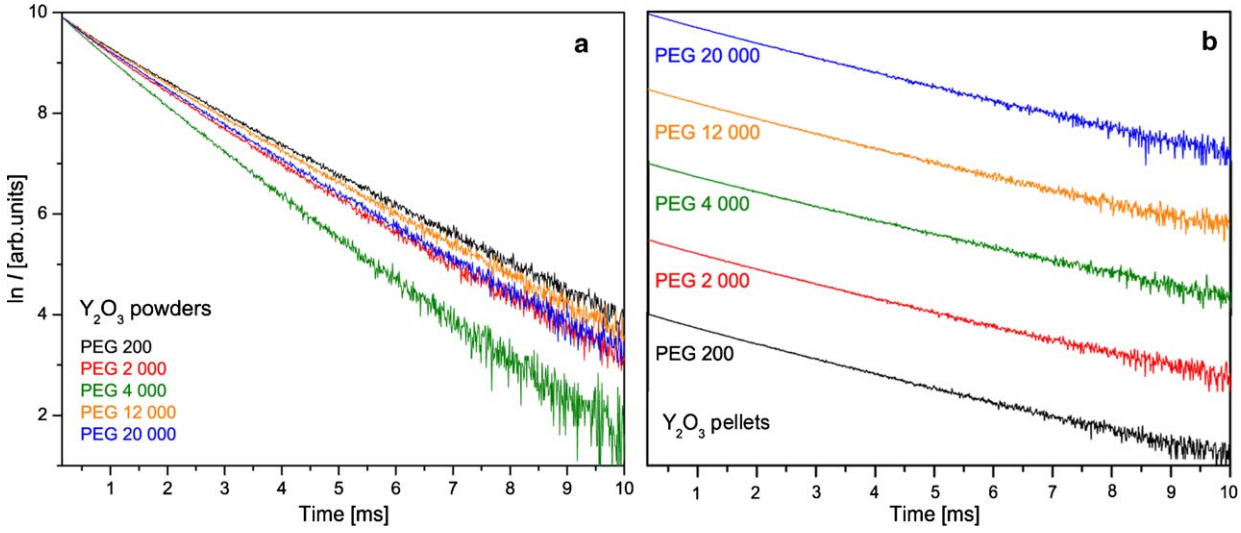

Fig. 4. Luminescence emission decay profiles for (a) Y_2O_3:Eu^{3+} powder and (b) pellet samples of the $^5D_0$ emitting level obtained under excitation of 467 nm (λ_{em} = 611 nm). (For interpretation of the references to color, the reader is referred to the web version of the article.)

values are given in the Tables 1 and 2. For all samples fluorescence decay profiles were adjusted by a single-exponential function showing that a single step radiative deexcitation process was present. Obtained relatively high lifetime values of about 1.5 ms are characteristic of europium species with a low non-radiative energy transfer probability. However, lower lifetime of about 1.1 ms, similar to those reported for bulk Y_2O_3 [16], was observed for all ceramic samples.

It is well known that excited states relaxation occurs via two competitive paths: by light emission and by phonon emission. The rate of phonon emission, w, depends on the number of phonons emitted simultaneously to bridge the energy gap and is expressed as:

$$w \sim \exp\left(\frac{-k\,\Delta E}{h\nu_{\max}}\right) \tag{2}$$

where ΔE is the energy gap to the nearest lower level and $h\nu_{\max}$ is the maximum energy of phonons coupled to the emitting states. The phonon emission rate, w, decreases rapidly with an increase in ΔE, so that the competitive light emission becomes dominant [17]. Thus, the well-known high luminescence efficiency for $^5D_0$ level of Eu^{3+} is based on a large energy gap of more than 10^4 cm^{-1} that needs to be bridged to the next lower level of this ion.

The observed decay times (τ_{obs}) of the excited $^5D_0$ states of Eu^{3+} ions can be expressed according to the following equation:

$$\tau_{obs}^{-1} = \tau_R^{-1} + \tau_{NR}^{-1} \tag{3}$$

where τ_R and τ_{NR} represent radiative and non-radiative decay times, respectively.

Since Eu^{3+} ions possess distinguished electronic energy levels and radiative decay dominates as a result of minimized multiphonon decay, we would expect similar lifetime of $^5D_0$ state in both ceramic and nanopowder samples. From our results it was clear that this was not the case and an alternative explanation was sought. Meltzer and co-workers [18] observed a similar phenomenon in monoclinic Y_2O_3:Eu^{3+} and explained that behavior due to changes produced by the medium surrounding the nanocrystals which size was much smaller than the excitation wavelength. In this case the local electric field acting on the Eu^{3+} ion was determined by the combined effect of the Y_2O_3 medium contained within nanocrystals and that of the medium filling the voids.

The radiative lifetime of electric dipole transitions, τ_R, of an ion embedded in a medium could be expressed by following formula [18]:

$$\tau_R \sim \frac{1}{f(\mathrm{ED})}\,\frac{\lambda_0^2}{[1/3(n^2+2)]^2 n} \tag{4}$$

where f(ED) is the oscillator strength for the electric dipole transition, λ_0 is the wavelength in vacuum and n is the refractive index of the medium. The dependence of τ_R on the refractive index n, was caused by the change in the density of states for the photons in a medium of reduced light velocity and the modification of the polarizability of the surrounding medium. In the case where the particle size of the nanocrystals is considerably smaller than the wavelength of light, the refractive index n, should be replaced by n_{eff}, the effective refractive index, which is the function of the refractive index of the corresponding bulk material and refractive index of the particle surrounding medium [18]:

$$n_{\mathrm{eff}}(x) = x n_{\mathrm{bulk}} + (1-x) n_{\mathrm{med}} \tag{5}$$

where x represents the "optical filling factor", which shows fraction of space occupied by the nanoparticles, n_{bulk} is the value of refractive index of corresponding bulk material (in our case $n_{bulk} = n_{Y_2O_3} = 1.91$) and n_{med} is the refractive index of the medium surrounding the nanocrystals (in our case it is air, n_{med} = 1).

From Eq. (4) one can derive nonlinear equation which gives link between emission lifetimes of $^5D_0$ state in bulk

Table 3
Calculated refractive index (n_{sample}) and "optical filling factor" (x_{sample}) for powder and ceramic Y_2O_3:Eu^{3+} samples.

	Powder PEG 200	Powder PEG 2000	Powder PEG 4000	Powder PEG 12,000	Powder PEG 20,000	Ceramic samples
n_{sample}	1.61	1.68	1.76	1.65	1.68	1.80
x_{sample}	0.68	0.75	0.83	0.71	0.75	0.88

and nanopowder with effective index of refraction of sample:

$$\frac{\tau_{bulk}}{\tau_{sample}}(n_{bulk}^2+2)^2 n_{bulk} = n_{sample}^5 + 4n_{sample}^3 + 4n_{sample} \quad (6)$$

Then, the solution of this equation can be introduced in Eq. (5) for calculation of the optical filling factor in the following way:

$$x_{sample} = \frac{n_{sample} - n_{med}}{n_{bulk} - n_{med}} \quad (7)$$

According to the Eqs. (6) and (7) and taking the value for the lifetime of bulk Y_2O_3:Eu^{3+}, τ_{bulk}, to be 0.9 ms [19] we calculated refractive index (n_{sample}) and "optical filling factor" (x_{sample}) for powder and ceramic samples and presented obtained data in Table 3.

These results show that effective refractive indexes are similar for powder samples prepared with PEG 200, 2000, 12000 and 20000, which is in a good agreement with their similar morphology as revealed from SEM images. Refractive index calculated for PEG 4000 sample differs and is similar with ceramic pellets indicating that observed "chunk" morphology is going toward bulk. Optical filling factor presents a measure of discrepancy between emission kinetics of bulk and nanomaterials, Eq. (5), and the obtained results, ranging from 0.68 to 0.88, follow the same trend found for the effective refraction index values. Powder obtained with PEG 4000 shows out of trend behavior and further investigations are necessary to explain this.

4. Conclusions

We demonstrated a successful procedure, based on the PEG – assisted combustion synthesis, for the fabrication of pure phase, nanocrystalline Y_2O_3:Eu^{3+} powders. The difference in the morphology of obtained powders and ceramic pellets can be explained as a function of PEG molecular weight: using longer polymer chains resulted in a more dense powder structure and smaller grains in correspondent ceramics.

Pellet samples have lower asymmetry coefficient of the Eu^{3+} coordination environment then powder ones, which is a direct consequence of the structural consolidation due to the applied post-synthesis treatment – loading and annealing. Maximum splitting of Stark component is almost identical for both powder and pellet samples, showing equal strength of the crystal field acting on europium ions and no change in the Eu–O distances. Rather high lifetime values in both types of samples are characteristic of europium species with low non-radiative energy transfer probability while observed lifetime lengthening compared to the bulk material is consistent with the theory of effective medium representation of refractive index in nanophosphors. Lifetime values observed for pellets are in accordance with the grain growth and material densification, and are similar with those found in the literature for the bulk Y_2O_3:Eu^{3+}. Luminescence measurements showed that the ceramic samples retained good optical properties of the starting nanocrystalline Y_2O_3:Eu^{3+} powder.

Acknowledgements

Authors acknowledge the financial support of the Ministry of Science of the Republic of Serbia (Project 142066). R.M. Krsmanović is also thankful to the NATO support in the realization of this experiment (grant reference number CBP.EAP.RIG.983373).

References

[1] O.A. Lopez, J. McKittrick, L.E. Shea, Fluorescence properties of polycrystalline Tm^{3+}-activated $Y_3Al_5O_{12}$ and Tm^{3+}–Li^+ co-activated $Y_3Al_5O_{12}$ in the visible and near IR ranges, J. Lumin. 71 (1997) 1–11.
[2] B. Bihari, H. Eilers, B. Tissue, Spectra and dynamics of monoclinic Eu_2O_3 and Eu^{3+}:Y_2O_3 nanocrystals, J. Lumin. 75 (1997) 1–10.
[3] R. Schmechel, M. Kennedy, H. von Seggem, H. Winkler, M. Kolbe, R. Fisher, L. Xaomao, A. Benker, M. Winterer, H. Hahn, Luminescence properties of nanocrystalline Y_2O_3:Eu^{3+} in different host materials, J. Appl. Phys. 89 (2001) 1679–1686.
[4] P. Majewski, M. Rozumek, H. Schluckwerder, F. Aldinger, Phase diagram studies in the systems La_2O_3–SrO–Ga_2O_3 and La_2O_3–MgO–Ga_2O_3 at 1400 °C in air, Int. J. Inorg. Mater. 3 (2001) 1343–1344.
[5] A. Garcia-Murillo, C. Luyer, C. Garapon, C. Dujardin, E. Bernstein, C. Pedrini, J. Mugnier, Optical properties of europium-doped Gd_2O_3 waveguiding thin films prepared by the sol–gel method, Opt. Mater. 19 (2002) 161–168.
[6] W. Jungowska, Phase equilibria in the system La_2O_3–K_2O–P_2O_5, J. Thermal Anal. Calorimetry 60 (2000) 193–197.
[7] M.Z. Su, W. Yhao, Rare earths ions in advanced X-ray imaging materials, in: L. Guokui, J. Bernard (Eds.), Spectroscopic Properties of Rare Earths in Optical Materials, Springer-Verlag, Berlin/Heidelberg, 2005, p. 521.
[8] P.S. Anil Kumar, J.J. Shrotri, S.D. Kulkarni, C.E. Deshpande, S.K. Date, Low temperature synthesis of $Ni_{0.8}Zn_{0.2}Fe_2O_4$ powder and its characterization, Mater. Lett. 27 (1996) 293–296.
[9] A. Lessing Paul, Mixed-cation oxide powders via polymeric precursors, Ceram. Bull. 68 (1989) 1002–1007.
[10] Y.P. Fu, S. Tsao, C.T. Hu, Preparation of $Y_3Al_5O_{12}$:Cr powders by microwave-induced combustion process and their luminescent properties, J. Alloy Compd. 395 (2005) 227–230.
[11] Y.P. Fu, S. Tsao, C.T. Hu, Y.D. Yao, Microwave-induced combustion synthesis of $Li_{0.5}Fe_{2.5-x}M_xO_4$ (M = Al, Cr, Mn) powder and their characterization, J. Alloy Compd. 395 (2005) 272–276.
[12] R.W. Cheary, A.A. Coelho, A fundamental parameters approach to X-ray line-profile fitting, J. Appl. Crystallogr. 25 (1992) 109–121.
[13] M. Mitric, P. Onnerud, D. Rodic, R. Tellgren, A. Szytula, M.Lj. Napijalo, The preferential site occupation and magnetic properties of $Gd_xY_{2-x}O_3$, J. Phys. Chem. Solids 54 (1993) 967–972.

[14] Ž. Andrić, M.D. Dramićanin, M. Mitrić, A. Bessière, B. Viana, Polymer complex solution synthesis of $(Y_xGd_{1-x})_2O_3:Eu^{3+}$ nanopowders, Opt. Mater. 30 (2008) 1023–1027.
[15] O.L. Malta, E. Antic-Fidancev, M. Lemaitre-Blaise, A. Milicic-Tang, M. Taibi, The crystal field strength parameter and the maximum splitting of the $^7F_1$ manifold of the Eu^{3+} ion in oxides, J. Alloy Compd. 228 (1995) 41–44.
[16] R. Schmechel, H. Winkler, L. Xaomao, M. Kennedy, M. Kolbe, A. Benker, M. Winterer, R.A. Fischer, H. Hahn, H. von Seggern, Photoluminescence properties of nanocrystalline $Y_2O_3:Eu^{3+}$ in different environments, Scripta Mater. 44 (2001) 1213–1217.
[17] E. Nakazawa, Phosphor Handbook, RC Press, Boca Raton, 1999.
[18] R.S. Meltzer, Dependence of fluorescence lifetimes of $Y_2O_3:Eu^{3+}$nanoparticles on the surrounding medium, Phys. Rev. B 60 (1999) R14012.
[19] X.Y. Chen, Comparison of the lifetimes of the $^5D_0$ and $^5D_1$ states of Eu^{3+} between $Eu:Y_2O_3@Al_2O_3$ nanocrystals and bulk crystalline $Eu:Y_2O_3$ crystal, in: E.V. Dirote (Ed.), Nanotechnology Focus, Nova Science Publishers, New York, 2005, pp. 141–173.